Reprinted from JOURNAL OF CLIMATE, Vol. 6, No. 4, April 1993
American Meteorological Society

Case Studies of Extreme Climatic Events in the Amazon Basin

JOSE A. MARENGO* AND STEFAN HASTENRATH

Department of Meteorology, University of Wisconsin, Madison, Wisconsin

(Manuscript received 23 August 1991, in final form 22 July 1992)

ABSTRACT

The mechanisms of climate anomalies in the Amazon basin were explored from surface climatological and hydrological series, upper-air, and satellite observations. The paper is focused on the March–April rainy season peak in the northern portion of Amazonia. Case studies for the moderately wet year 1986 (WET), showed a relatively far-southerly location of the Atlantic near-equatorial trough, and embedded intertropical convergence zone (ITCZ); strong ascending motion and vigorous convection over the Amazon basin, contrasting with pronounced subsidence off the west coast of South America; and weak subtropical westerly jets (STWJ) in both hemispheres. In contrast, the extremely dry El Niño year 1983 (DRY), featured a more northward located ITCZ; subsidence over the Amazon basin; ascending motion and convective rainfall to the west of the Andes; and strong STWJ.

In synthesis from these analyses, some major mechanisms of extreme rainfall events in northern Amazonia stand out, but only for the late austral summer, when the ITCZ in the tropical Atlantic–South American sector attains its southernmost position, as the intense summertime convection over Amazonia is an important component of the ITCZ. Thus, ascending motion over the northern part of the Amazon basin with an anomalously far-southward displaced ITCZ appears compatible with subsidence to the west of the Andes during the high phase of the Southern Oscillation (SO), which is defined by anomalously high/low pressure at Tahiti/Darwin. In contrast, ascending motion and convection over the easternmost equatorial Pacific, as is common during extreme events of the low-SO phase, require compensatory subsidence, and this may interfere with convection to the east of the Andes. However, hydrometeorological anomalies in Amazonia are not prevailingly related to the SO.

1. Introduction

As one of the three quasi-permanent centers of intense convection embedded in the equatorial trough zone, the Amazon basin may play a pivotal role in the functioning of the global climate system. The copious rainfall feeds the largest freshwater stream of the world. The associated abundant latent heat release makes the overlying atmospheric column one of the most powerful fuel boxes of the general circulation. The Amazon jungle owes its existence in part to this generous precipitation, and in turn plays a role of its own in the terrestrial–atmospheric hydrological cycle. Deforestation as a result of human activities in the course of recent decades is altering the conditions at the lower boundary of the atmosphere. Concern about this human interference is manifold (reviews in Salati et al. 1979; Hastenrath 1991; Dickinson 1986). With the prospects of such long-term modifications to the global climatic system caused by interference with the Amazon biosphere, the current functioning of the atmosphere–land–ocean system in the equatorial Americas is of crucial interest as a reference against which future evolutions may be compared. Beyond the description of the average annual cycle of circulation and climate over the region, an understanding is needed of the general circulation mechanisms involved in the "natural" climatic variability in the Amazon basin. Drawing on comprehensive observational evidence comprising conventional surface meteorological and hydrological series, satellite-derived estimates of tropical convection, and global upper-air analyses, this paper presents case study analyses of circulation characteristics for two contrasting extreme years in the Amazon basin.

2. Observations and data analysis

The database for this study consists of surface hydrometeorological data, satellite estimates of tropical convection, sea surface temperature (SST) taken from the Comprehensive Ocean Atmospheric Data Set (COADS), and global near-surface and upper-air analyses from the European Centre for Medium-Range Weather Forecasts (ECMWF).

Monthly rainfall totals at stations in tropical South America were collected for the period 1961–87. The

* Current affiliation: National Research Council, National Aeronautics and Space Administration/Goddard Institute for Space Studies, New York, New York.

Corresponding author address: Stephan Hastenrath, Department of Meteorology, University of Wisconsin, 1225 West Dayton Street, Madison, WI 53706.

spatial distribution of precipitation regimes throughout tropical Brazil has been variously described (Kousky 1980; Molion 1987; Rao and Hada 1990; Figueroa and Nobre 1990; Obregón and Nobre 1990; Nobre et al. 1991; Meste 1991). The largest annual precipitation totals are found within the domain indicated in Fig. 1 (Figueroa and Nobre 1990; Meste 1991) and the rainfall maximum occurs around March–April with a slightly later peak at stations in the north. A companion study (Marengo 1992) drawing on long-term observations also showed that surface circulation departures in the tropical Atlantic sector tend to be most distinct around March–April. Accordingly, a March–April rainfall index for Northern Amazonia (NAR), was compiled from 18 stations in this area (Fig. 1). The index NAR is the all-station average normalized departure from the 1967–86 mean of 7.4 mm per day (Fig. 2a). Within the domain of NAR (delineated in Fig. 1), a major rainfall maximum can be distinguished in the west separate from a minor nucleus near the mouth of the Amazon during March–April (Meste 1991; Fig. 5 in Figueroa and Nobre 1990). For the latter, diurnal circulations have been recognized as a major factor (Kousky 1980).

As further hydrometeorological information, water-level series were obtained from the Departamento Nacional de Aguas e Energia Elétrica (DNAEE), Brazil, for the gauging sites at Manaus on the Rio Negro, Óbidos on the Amazon, Manacapurú on the Solimões, and Santarém and Itaituba on the Tapajós (Fig. 1). From these, indices were constructed for the May–June–July season of maximum water level (apparent from the DANEE data), as normalized departures from the 1967–87 mean. The delay of the maximum water level reflects the hydrological lag with respect to the core of the rainy season.

The highly reflective cloud (HRC) dataset is the record of subjectively identified areas of large-scale or-

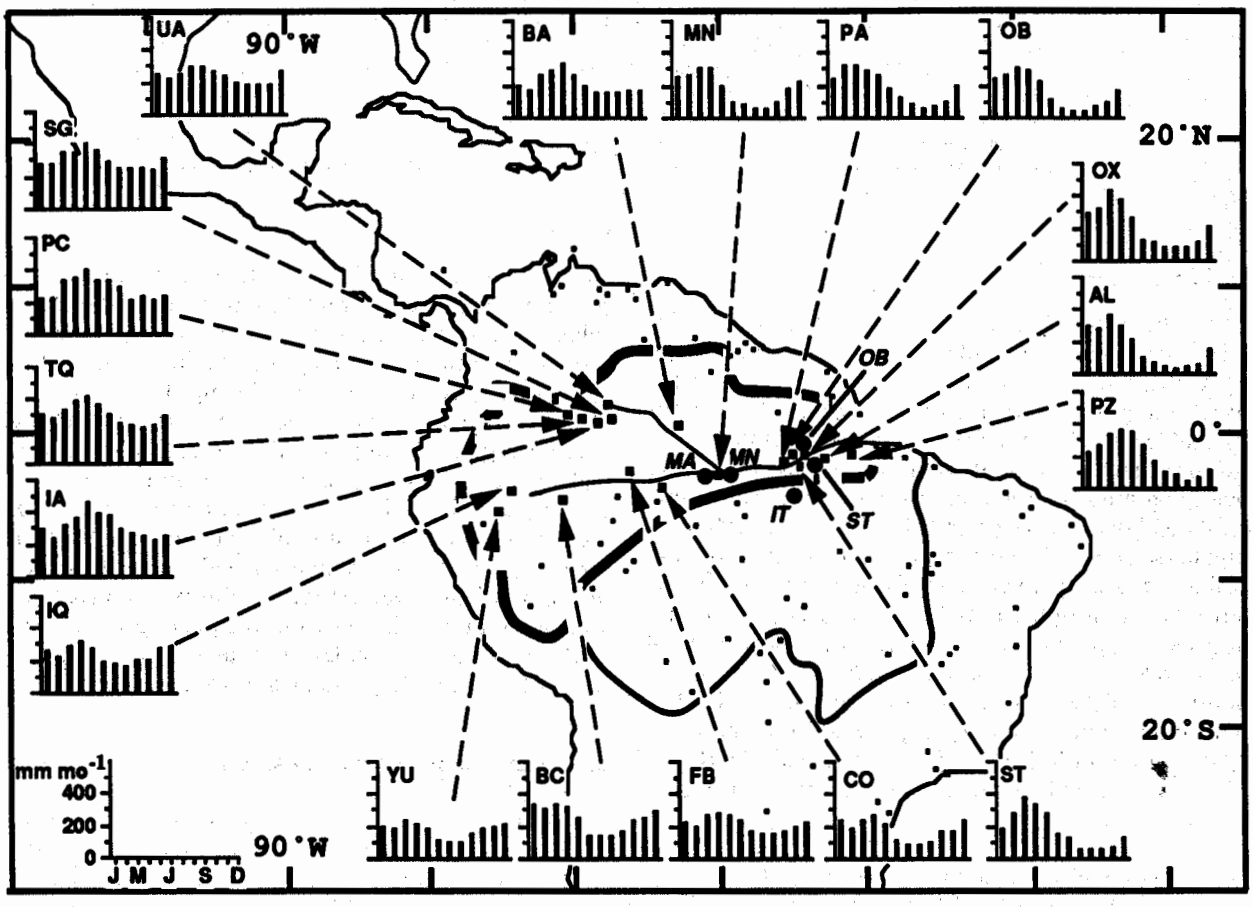

FIG. 1. Orientation map of rainfall stations and regimes. Thin solid line delineates Amazon catchment, and heavy solid line domain for which rainfall index NAR was compiled from the 18 raingage stations indicated by large dots and annual cycle diagrams, namely: Uaupes (UA), São Gabriel da Cachoeira (SG), Taraqua (TQ), Iauareté (IA), Iquitos (IQ), Yurimaguas (YU), Benjamín Constant (BC), Fonte Boa (FB), Coari (CO), Santarém (ST), Porto de Moz (PZ), Altamira (AL), Oriximina (OX), Óbidos (OB), Parintis (PA), Manaus (MN), Barcelos (BA). Raingage stations outside the NAR domain are entered as small dots without letter symbols. Also shown by large dots are the river gauging sites of Rio Negro at Manaus (MN), Solimões at Manacapurú (MA), Amazon at Óbidos (OB), and Tapajós at Santarém (ST) and Itaituba (IT).

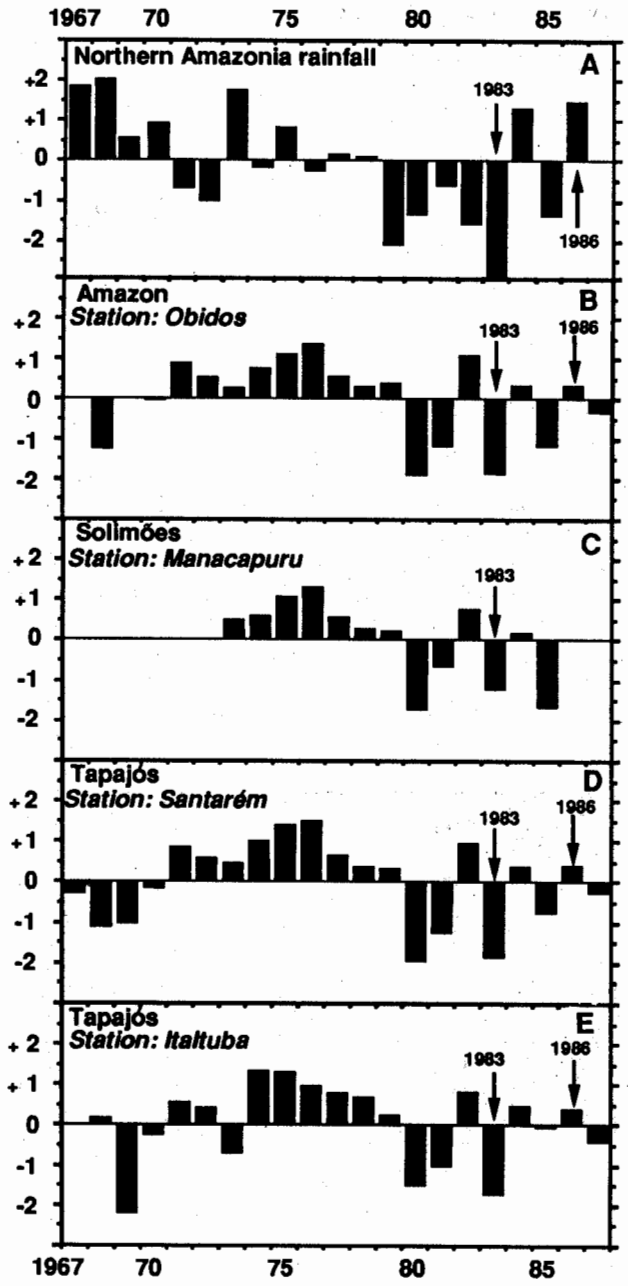

FIG. 2. Time series of rainfall in northern Amazonia and May–July water-level indices for the Amazon basin. Arrows indicate 1983 and 1986. See Fig. 1 for domain of rainfall index and locations of river gauging sites (DNAEE 1989). (a) Rainfall index NAR for Northern Amazonia (normalized departures from 1967–86 mean of 7.4 mm day^{-1}, standard deviation of 0.6 mm day^{-1}), from raingage network; (b) water-level index of the Amazon (normalized departures from 1967–87 mean of 443 cm, standard deviation of 53 cm, at Óbidos, 01°54′S, 54°30′W) for May–July; (c) water-level index of the Solimões river (normalized departures from 1967–87 mean of 620 cm, standard deviation of 99 cm, at Manacapurú, 03°13′S, 60°35′W) for May–July; (d) water-level index of the Tapajós river (normalized departures from 1967–87 mean of 345 cm, standard deviation of 45 cm, at Santarém, 02°35′S, 54°43′W) for May–July; (e) water-level index of the Tapajós river (normalized departures from 1967–87 mean of 487 cm, standard deviation of 53 cm, at Itaituba, 04°16′S, 55°58′W) for May–July;

ganized daytime convection on Mercator projection mosaics (Garcia 1985; Hastenrath 1990a). They are composed of many individual convective cells known as cumulus clusters. For the band 25°N–25°S, counts of days with HRC were made for 1°-square areas, and then combined into 5°-square areas. The measurements of outgoing longwave radiation (OLR) from scanning radiometers carried aboard National Oceanic and Atmospheric Administration (NOAA) polar orbiting satellites were compiled with a 2.5°-lat–long resolution (Janowiak et al. 1985; Gruber et al. 1987).

The SST for the tropical Atlantic and eastern Pacific were extracted from the COADS dataset for the band 30°N–30°S and averaged for 2°-square areas. For details about the COADS set, refer to Slutz et al. (1985) and Oort et al. (1987).

The ECMWF global upper-air analyses for the years 1980–87 were obtained from the National Center for Atmospheric Research (NCAR), Boulder, Colorado. We used here the 1000- and 200-mb topography and wind fields, and the 500-mb vertical velocity. The archived vertical velocity is calculated from the surface pressure and initialized horizontal winds on model levels by solving the continuity equation. The analysis procedures used at ECMWF, the occasional changes in these procedures, and the biases in the analysis and background data are described in Trenberth and Olson (1988) and Hoskins et al. (1989).

3. Interannual variability of rainfall and river levels

Figure 2 illustrates the variation of hydrometeorological conditions in the Amazon basin over recent decades, from raingage measurements and river-level records. These figures show an era of wetter climate in the 1970s, with a change to prevailingly drier years in the past decade. During the 1980s, for which the ECMWF global upper-air analyses are available, the raingage and river records consistently indicate the El Niño year 1983 as extremely dry, and 1984 and 1986 as much wetter by comparison.

For the case study analysis of contrasting years, the extremely dry El Niño year 1983 (DRY), was the obvious candidate to illustrate dry conditions. Regarding a counterpart year with more nearly average conditions, 1984 has been studied before (Philander 1986; Kayano et al. 1988) in different context and for different seasons, and found to be a somewhat unusual year. Moreover, the raingage records in the northern and eastern portions of the Amazon basin (Fig. 2a) indicate that March–April 1986 was if anything somewhat wetter than 1984. On balance, 1986 (WET) was chosen to represent the wet case. Evidence for the contrasting years 1986 and 1983 are presented in Table 1, Fig. 3, and Figs. 5–7. To complement these analyses, Figs. 4 and 8 also offer a limited comparison of the 1983 with the 1984 conditions.

For the chosen WET and DRY events, Table 1 summarizes the seasonal evolution of Rio Negro water lev-

TABLE 1. Seasonal evolution of departures of Rio Negro water level, in cm, and of Manaus rainfall, in mm, during WET event 1985–86 and DRY event 1982–83.

	Rio Negro level (cm)			Manaus rain (mm)		
Season	WET	DRY	Mean (1903–87)	WET	DRY	Mean (1941–88)
Sep–Oct	+146	+88	2060	+64	−31	100
Nov–Dec	+187	+88	1879	+2	+44	202
Jan–Feb	+235	+78	2184	+37	−193	261
Mar–Apr	+41	−162	2455	+19	−101	325
May–Jun	+60	−101	2716	+30	−49	184

els and of rainfall at Manaus (Fig. 1). Anomalously high stands of water level began in September–October 1985 and grew largest in January–February 1986. In 1983, rainfall deficiencies became most pronounced during January–February, while the deficit of the water level continued to aggravate to March–April.

4. Circulation and convection over the tropical Americas

This section is devoted to the detailed case study analysis of March–April circulation in the representative WET year 1986 and DRY year 1983 in Amazonia, with a limited comparison of 1983 versus 1984 conditions. In addition to surface marine and continental hydrometeorological records, the study relies on analyses of the upper-air circulation and satellite measurements of tropical convection. Thus it meaningfully complements a companion paper (Marengo 1992), confined to surface information but spanning the past four decades.

a. Sea surface temperature

The March–April SST conditions during two contrasting years are documented in Fig. 3, with Fig. 3a referring to 1986 WET, Fig. 3b to 1983 DRY, while Fig. 3c maps the difference between the two years. Together, the three panels of Fig. 3 reveal for the extreme El Niño year 1983, as compared to the more nearly average year 1986, considerably warmer waters not only in the equatorial eastern Pacific but also in a broad band extending from the Caribbean across the tropical North Atlantic. In detail, the zone of warmest surface waters is located distinctly farther south in 1986 (Fig. 3a) as compared to 1983 (Fig. 3b). The SST difference pattern 1984 minus 1983 (Fig. 4b) resembles Fig. 3c in showing negative values in the equatorial Pacific and most of the tropical North Atlantic, contrasting with positive values in the south Atlantic. These characteristics of the SST distribution in the selected years are consistent with the companion paper on the interannual variability in the past four decades, and are further relevant to the circulation of the lower atmosphere, to be discussed in the following section.

b. Near-surface circulation

Figure 5 displays the 1000-mb geopotential height (Figs. 5a,b,c) and wind field (Figs. 5d,e,f). During WET (Fig. 5a) as compared to DRY (Fig. 5b), the North Atlantic subtropical high is stronger, the south Atlantic high weaker, the enclosed near-equatorial low-pressure trough is located farther south, and concomitant with these features the meridional pressure gradient appears steepened over the low-latitude North Atlantic, but reduced to the south of the equator. All of these characteristics of the contour/pressure fields

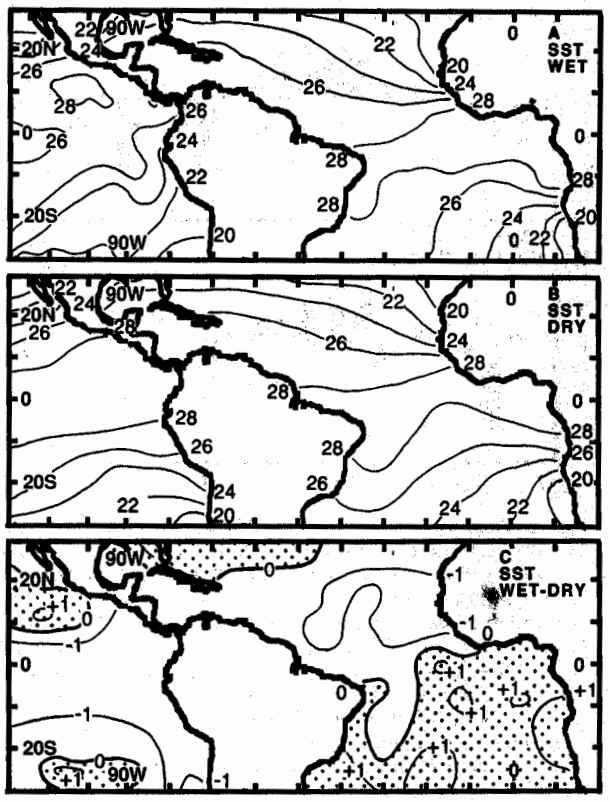

FIG. 3. Sea surface temperature in (a) March–April 1986 WET, contour interval 2°C; (b) March–April 1983 DRY, contour interval 2°C; (c) WET–DRY, zero line heavy, contour interval 1°C, positive areas indicated by dot raster.

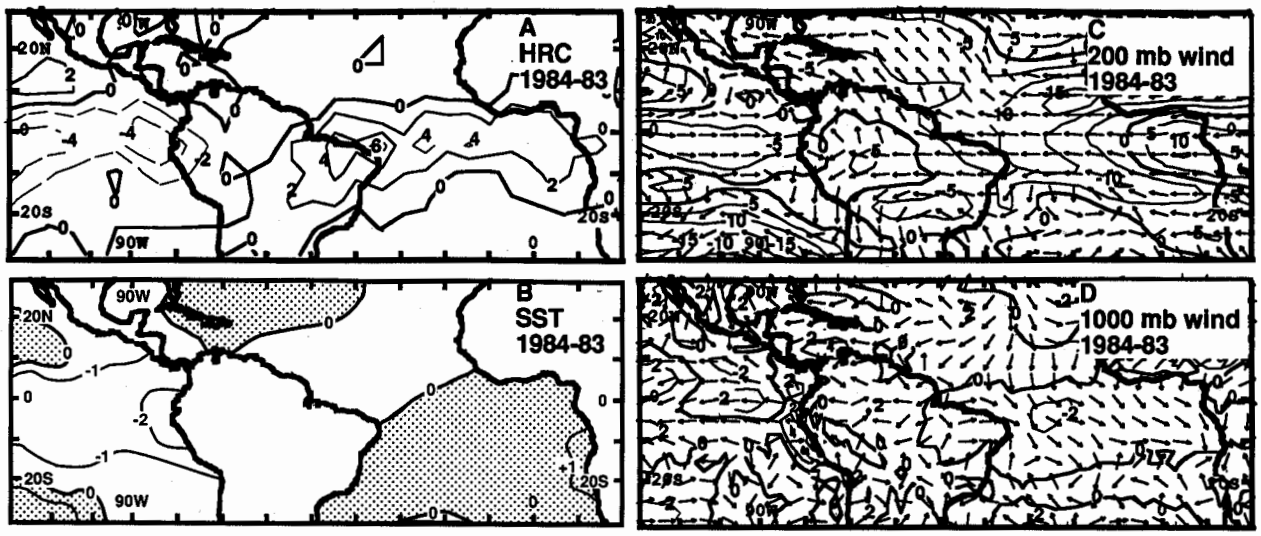

FIG. 4. Difference maps, March–April 1984 minus 1983; (a) highly reflective clouds HRC in days; (b) sea surface temperature SST, contour interval 2°C; (c) 200-mb wind, isotach spacing 5 m s^{-1}; (d) 1000-mb wind, isotach spacing 2 m s^{-1}.

are concordant with the salient features of the SST patterns described in section 4 and Fig. 3, namely the colder tropical North Atlantic and the more southerly position of the zone of warmest surface waters during WET (Fig. 3a) as compared to DRY (Fig. 3b).

The 1000-mb wind fields during the two contrasting

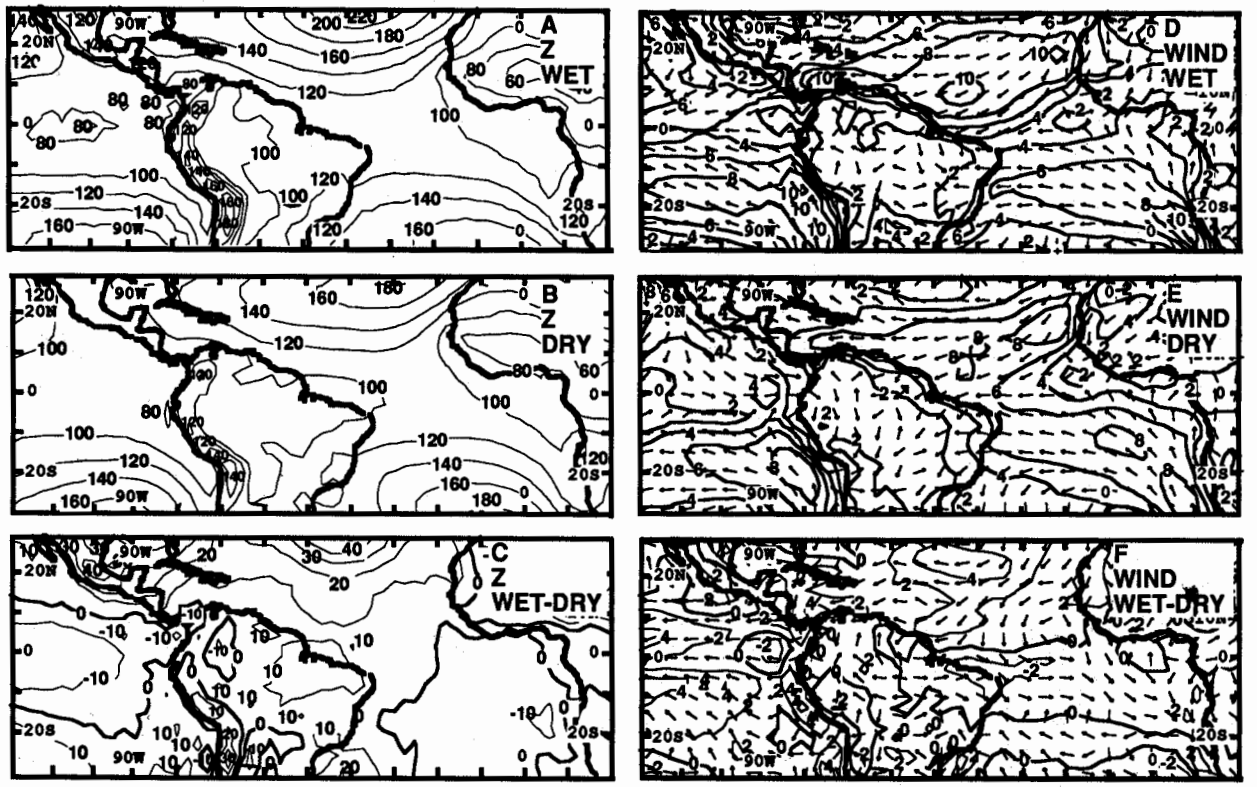

FIG. 5. 1000-mb circulation patterns during March–April 1986 WET [(a), (d)], March–April 1983 DRY [(b), (e)], and the difference WET minus DRY [(c), (f)]: (a) 1000-mb geopotential height, in gpm, WET, (b) 1000-mb geopotential height, in gpm, DRY, (c) WET–DRY 1000-mb geopotential height, in gpm, (d) 1000-mb wind, in m s^{-1}, WET, (e) 1000-mb wind, in m s^{-1}, DRY, (f) WET–DRY 1000-mb wind, in m s^{-1}. The contour intervals are 2 m s^{-1} for the wind in (d), (e), (f), 20 gpm for geopotential height in (a), (b), and 10 gpm in (c). Zero line heavy in (c, f).

extreme years (Figs. 5d,e,f) broadly agree with the contour patterns (Fig. 5a,b,c). Thus during WET as compared to DRY, the North Atlantic trades appear accelerated and the southeast trades appear reduced (Fig. 5d,e,f), consistent with the steepened meridional pressure gradient over the North Atlantic and the weakened gradients south of the equator (Fig. 5a,b). Indeed, the difference map, Fig. 5f, shows nicely the stronger northeast trades during WET as compared to DRY, and northwesterly difference vectors in the realm of the southeast trades of the south Atlantic! In accordance with the varying intensity of the trades over the two hemispheres, the Atlantic near-equatorial wind confluence is located distinctly farther south in WET than in DRY (Fig. 5d and f). Over the eastern equatorial Pacific, there are some further noteworthy features in the near-surface wind field: while 1986 WET (Fig. 5d) shows the usual pattern of strong easterlies, a characteristic of the extreme 1983 El Niño year (Fig. 5e) was the appearance of surface westerly winds over a broad zone of the equatorial Pacific. This extremely anomalous event also dominates the difference map, Fig. 5f. The wind difference pattern 1984 minus 1983 (Fig. 4d) is similar to Fig. 5f for 1986 minus 1983. This case study analysis is consistent with the surface circulation characteristic of anomalous rainy seasons in the Amazon basin derived from long-term data sources (Marengo 1992).

Complementing the 1000-mb contour and flow patterns in Fig. 5, Fig. 6 maps the divergence of the near-surface wind field (Fig. 6a,b,c). Consistent with a more southerly location of the wind confluence (Fig. 5d,e), the near-equatorial band of maximum convergence in the Atlantic–South American sector is found farther south and appears more intense in WET (Fig. 6a) than in DRY (Fig. 6b). This contrast between WET and DRY is further illustrated in Fig. 6c.

c. *Upper-air circulation*

Figure 7 maps the 200-mb wind (Figs. 7a,b,c) and the 500-mb vertical motion patterns (Figs. 7d,e,f). During WET (Fig. 7a) as compared to DRY (Fig. 7b) the subtropical westerly jets (STWJ) of both hemispheres appear relatively weak and displaced poleward. During WET (Fig. 7a), westerlies are found over the eastern equatorial Pacific, while easterlies prevail over the eastern equatorial Atlantic, and there is an indication of the Bolivian–Peruvian upper-tropospheric anticyclone. In contrast, during DRY (Fig. 7b), the STWJ of both hemispheres appear accelerated and shifted equatorward; easterlies cover the eastern equa-

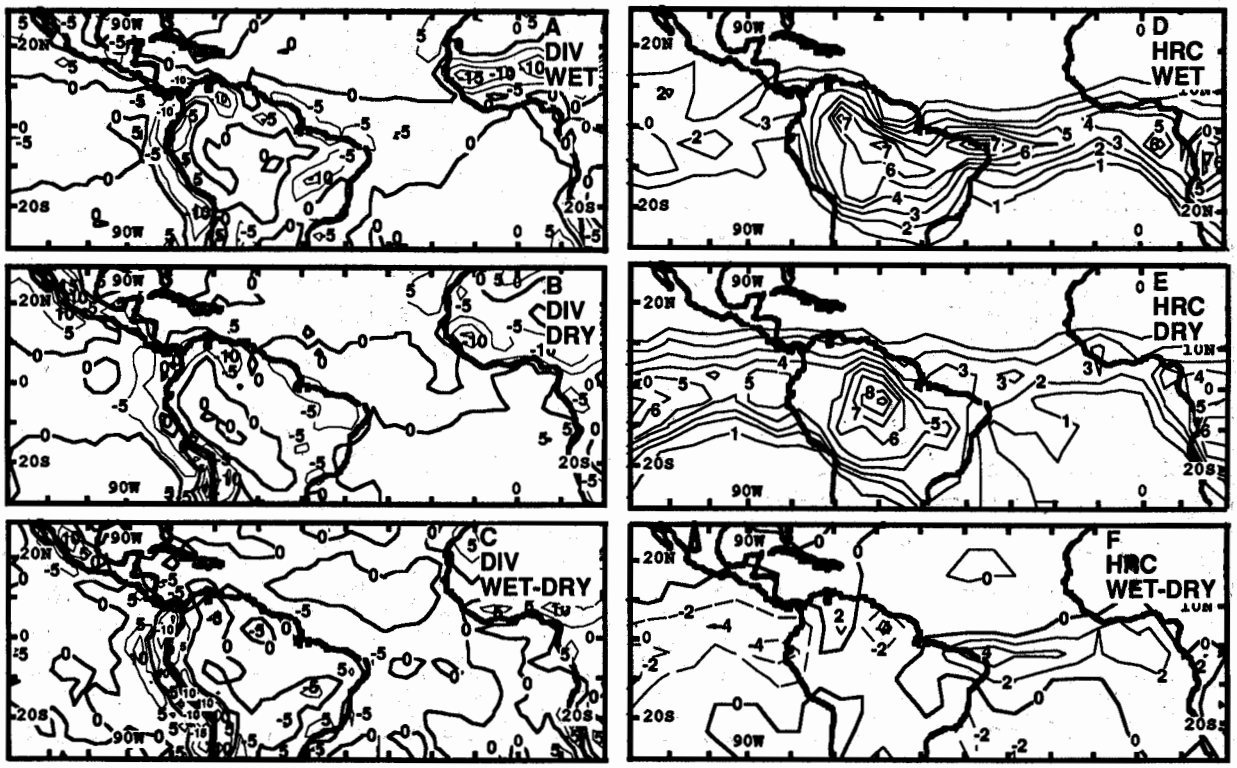

FIG. 6. Divergence in 10^{-6} s^{-1} at 1000 mb (a), (b), (c) and highly reflective clouds HRC in days (d), (e), (f) during March–April 1986 WET (a), (d), March–April 1983 DRY (b), (e), and the difference WET minus DRY (c), (f). (a) wind divergence WET, (b) wind divergence DRY, (c) wind divergence WET minus DRY, (d) HRC WET, (e) HRC DRY, (e) HRC WET minus DRY. Contour intervals are 5×10^{-6} s^{-1} for wind divergence (a), (b), (c), and two days for the HRC (d, e, f). Zero line heavy.

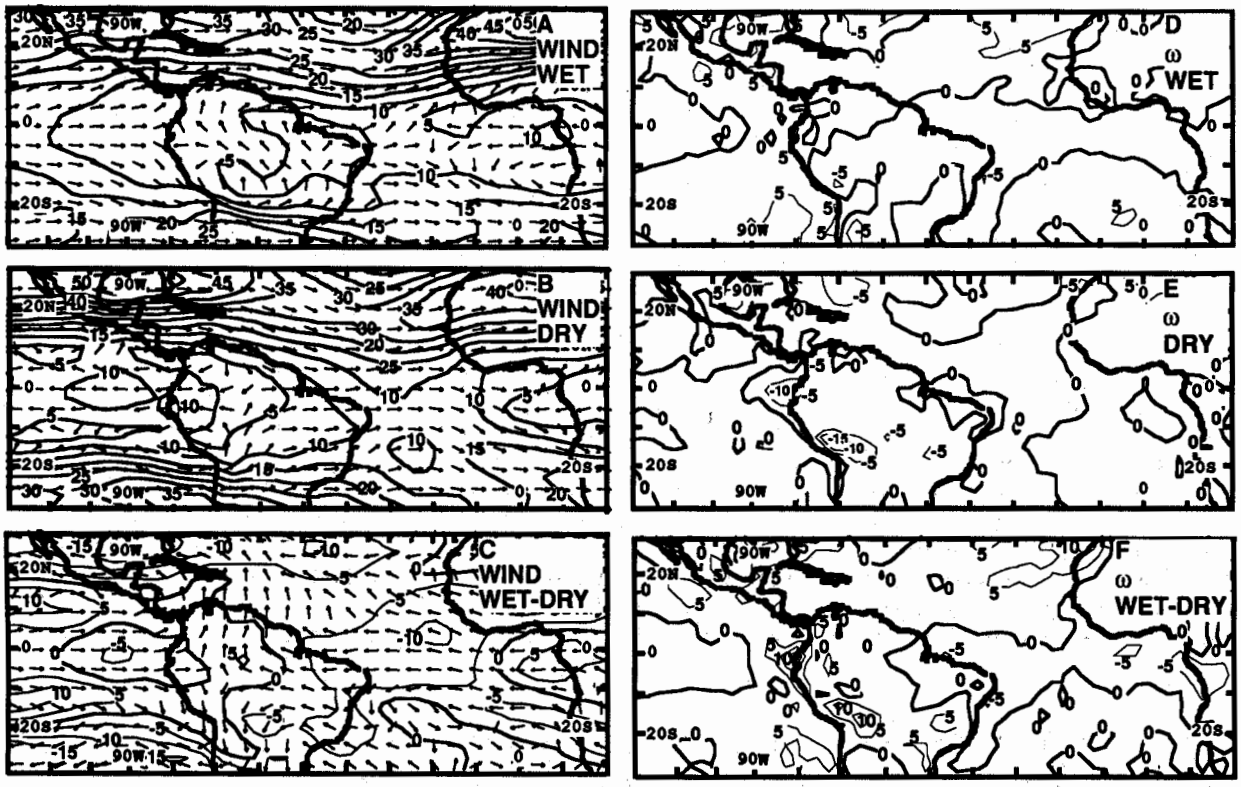

FIG. 7. Upper-tropospheric circulation during March–April 1986 WET (a), (d), March–April 1983 DRY (b), (e), and the difference WET minus DRY (c), (f): (a) 200-mb wind in m s^{-1}, WET, (b) 200-mb wind in m s^{-1}, DRY, (c) WET–DRY 200-mb wind in m s^{-1}, (d) 500-mb vertical velocity in 10^{-4} mb s^{-1}, WET, (e) 500-mb vertical velocity in 10^{-4} mb s^{-1}, DRY, (f) WET–DRY 500-mb vertical velocity in mb s^{-1}. Contour intervals are 5 m s^{-1} for the 200-mb wind speed in (a), (b), (c), and 5×10^{-4} mb s^{-1} for the 500-mb vertical velocity (in d), (e), (f). Zero line heavy in (d, e, f).

torial Pacific, while westerlies extend from the South American continent across the equatorial Atlantic into Africa, and the Bolivian–Peruvian upper-tropospheric anticyclone appears weakened and shifted westward. Another upper-tropospheric anticyclone is located over Panama, and the trough off Brazil is weak. The difference map, Fig. 7c, further highlights the contrasts between the two years, which are dominated by the unusual flow conditions of the extreme 1983 El Niño year with its anomalous easterly winds over the equatorial eastern Pacific, westerlies over the equatorial zone of the Atlantic, and accelerated STWJ. As with the lower-tropospheric circulation, the wind difference pattern 1984 minus 1983 (Fig. 4c) is similar to that for 1986 minus 1983 (Fig. 7c).

Some remarks seem in order on the variations of the STWJ. Accelerated jets around much of the globe are known to be typical of warm events in the Pacific or the low phase of the Southern Oscillation (SO) (Aceituno 1989; review in Hastenrath 1991, 282–288). One may conjecture that reduced convection over the Amazon basin would by itself be conducive to weak STWJ in the American sector, but this may be overcompensated by thermal influences from the upstream Pacific. In this spirit, STWJ variations related to the convective activity over South America deserve further study (Pedro Silva Dias, personal communication 1992).

The 500-mb vertical motion (Figs. 7d,e,f) exhibits patterns similar to the divergence in the 1000-mb wind field (Figs. 6a,b,c). The maps show for both years (Figs. 7d,e) ascending motion over much of the South American continent and in a band across the tropical Atlantic. However, this band appears broader, more organized, and located more to the south in WET as compared to DRY, in agreement with the band of maximum near-surface convergence (Figs. 6a,b,c) and the near-equatorial wind confluence (Figs. 5d,e). Highlighting the contrasts between the two years, the difference map, Fig. 7f, shows the largest negative values in a continuous band centered over the southern equatorial Atlantic.

d. Convection and rainfall

Figure 8 compares the precipitation distributions of the contrasting years as obtained from the raingage network on the South American continent, while Figs.

6d,e,f map the convective activity derived from satellite measurements of HRC over the broader sector from the eastern Pacific across the Americas and the Atlantic into tropical Africa. Charts constructed of OLR patterns provide similar information on tropical convection as HRC, and are not reproduced here.

For WET, as compared to DRY, Fig. 8 shows larger precipitation over a substantial portion of the NAR domain (Fig. 1), but also in a band extending from eastern Amazonia into northeast Brazil. This appears consistent with the findings of Moura and Kagano (1986), who called attention to the tendency for a considerable zonal extent of rainfall anomalies, at times stretching continuously from the eastern slope of the Andes, across the Amazon basin and northeast Brazil, into the equatorial Atlantic and Africa. The drought conditions in northeastern South America during 1983, in particular, have been variously noted (Aceituno 1988; Kayano et al. 1988; Hastenrath 1990b). While the raingage network shown in Fig. 1 does not completely cover the Pacific coastal regions of Ecuador and northern Peru, enhanced rainfall has been reported there for the 1983 El Niño (Kousky et al. 1984; Horel and Cornejo-Garrido 1986; Aceituno 1988; Kayano et al. 1988). The rainfall difference map 1984 minus 1983 (Fig. 8d) also shows positive values in a large portion of the Amazon basin, albeit with differences in the pattern detail.

Figures 6d–f, displaying the satellite measurements of HRC, afford a broader spatial perspective of large-scale organized convection than the precipitation maps (Fig. 8), limited as they are to the raingage network over the South American continent. The HRC maps (Fig. 6d,e) reveal for WET as compared to DRY a more southward-located, organized, intense near-equatorial convection band, a characteristic highlighted further in the difference maps (Fig. 6f). The HRC difference patterns 1984 minus 1983 (Fig. 4a) share the main characteristics of Fig. 6f for 1986 minus 1983. The contrast in the convection patterns between these two years is consistent with the broad zonally oriented band of abundant rainfall apparent over the Amazon Basin during WET as compared to DRY (Fig. 8a and d). These differences in large-scale organized convec-

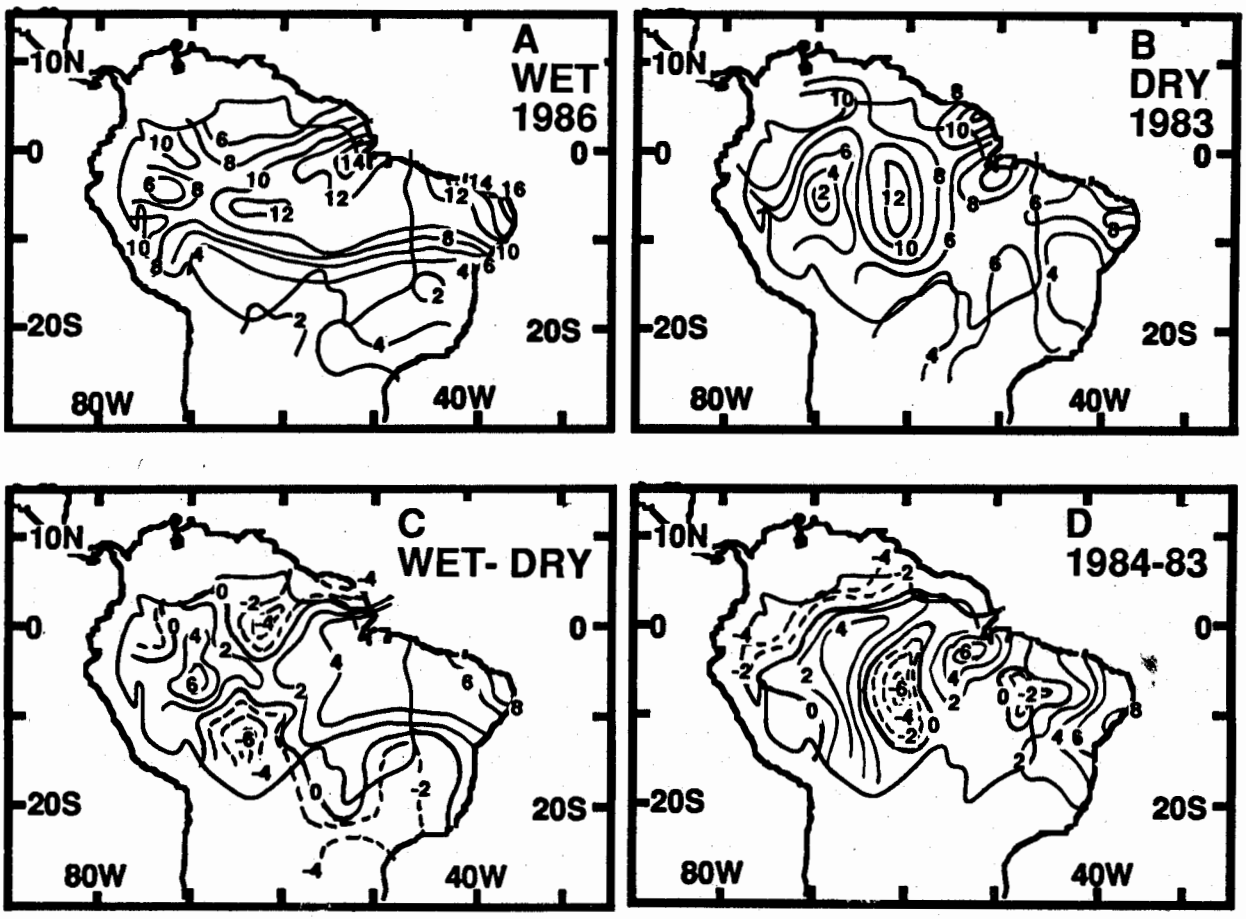

FIG. 8. March–April rainfall in the Amazon basin (mm per day): (a) 1986 WET, (b) 1983 DRY, (c) WET minus DRY (1986–1983), (d) 1984–1983. Zero line heavy, and negative values broken lines in (c), (d).

tion agree further with the analysis of the lower-tropospheric circulation discussed in section 4d, in particular the more southerly position of the Atlantic near-equatorial wind confluence (Figs. 5d and 5e), and the more southerly position and greater intensity of the band of convergence (Figs. 6a and 6b). In support of the early findings of Moura and Kagano (1986), Fig. 6f highlights the remarkable spatial coherence in the departures of tropical convection expanding from the Amazon basin, across Northeast Brazil and the equatorial Atlantic into the African continent.

5. Conclusions

The central theme of this study—the mechanisms of climate anomalies in the Amazon basin—appears particularly timely, because the region contains one of the major convection centers that drive the atmospheric circulation of the tropics, and because the changing lower-boundary conditions resulting from the progressive deforestation are feared to have substantial climatic consequences. With this motivation it was desirable to exploit the existing observational evidence. The sparse network of long-term raingage spread over this vast territory is deficient, even as complemented by some series of river water levels, but proved marginally sufficient to assess the rainfall distribution and regimes and to identify extreme events in the interannual variability of rainfall. The surface hydrometeorological data were complemented by satellite measurements of tropical convection. The ECMWF global upper-air analyses along with the ship SST observations were crucial for evaluating the ocean surface conditions and atmospheric circulation characteristics during the contrasting extreme years. This case study of upper-air circulation and convection complements a companion paper (Marengo 1992) on the mechanisms of interannual variability in Amazonia in the course of the past four decades as evidenced by surface observations.

Although the Amazon catchment comprises a vast area with precipitation during much of the year, convective rainfall is most abundant in a limited domain in the northern portion of the basin during mid- to late austral summer. The Amazon convection center of austral summer is an integral part of the ITCZ, which in this season reaches its southernmost location. In fact, the convective activity over the Amazon basin appears an important factor for the characteristic annual cycle in intensity and latitudinal migration of the ITCZ in the South American–tropical Atlantic sector (Hastenrath and Lamb 1977). Strong relationships between the large-scale circulation and regional rainfall are confined to the core of the rainy season in the northern portion of the basin around March–April.

The modern observational data banks available for the 1980s were used to advantage for detailed case studies of the contrasting extreme years 1986, which was moderately WET, and 1983, which was extremely DRY. It was found that the more copious rainfall occurs with a strong North Atlantic high, accelerated northeast trades, and colder North Atlantic but warmer south Atlantic waters. A preference for more abundant precipitation during the high phase of the SO is also indicated in Hastenrath et al. (1987): during March–April in the high-SO phase, the near-equatorial low-pressure trough and embedded ITCZ over the Atlantic sector tend to be displaced anomalously far southward, concomitant with a strengthened North Atlantic high and accelerated northeast trades, as well as anomalously cold North Atlantic and warm south Atlantic waters. It is noteworthy that a southward-displaced ITCZ and enhanced moisture import from the Atlantic associated with the accelerated Northeast trades, are conducive to more vigorous convection and rainfall over Amazonia. However, such circulation departure characteristics should not be regarded as limited to the high-SO phase. Rao and Hada (1990) reported moderate correlations of the SO with rainfall in various parts of Brazil.

In addition, these case studies provided a glimpse at anomalous upper-air circulations. In particular, during WET, there was vigorous upward motion and convection over Amazonia, and the STWJ of both hemispheres were weak. The upper-air flow during DRY was distinctly different: the Pacific coast of South America experienced ascending motion and convective rainfall, while subsidence prevailed over the Amazon basin. At the same time, the STWJ of both hemispheres were accelerated.

From these case study analyses, some major circulation mechanisms of rainfall anomalies in the Amazon basin can be proposed. These are synthesized in Figs. 9a–d. Thus, during WET (Fig. 9a and b), the North Atlantic high is strong, the meridional pressure gradient on its equatorward side steep, and the northeast trade-winds are accordingly accelerated. Consistent with the strong North Atlantic trades, the ITCZ is displaced southward. The Amazon convection center, being part of the ITCZ, is intensified. Further typical associations include anomalously cold surface waters in the tropical North Atlantic and negative SST departures south of the Equator. The features of the equatorial zonal circulation cells are illustrated in Fig. 9b. During WET in Amazonia, there is subsidence over the west coast of South America, while ascending motion and convection prevail over Amazonia. During DRY (Figs. 9c and d), circulation departures are broadly inverse to those in WET (Figs. 9a and b). Thus, the North Atlantic high is weak, as are the northeast trades, and the ITCZ remains north of its usual latitude position, entailing reduced convection over Amazonia. Similarly, the tropical North Atlantic is relatively warm, while the south Atlantic is unusually cold.

Some qualifications are in order regarding the synthesized schemes in Fig. 9. Thus the upper-air circu-

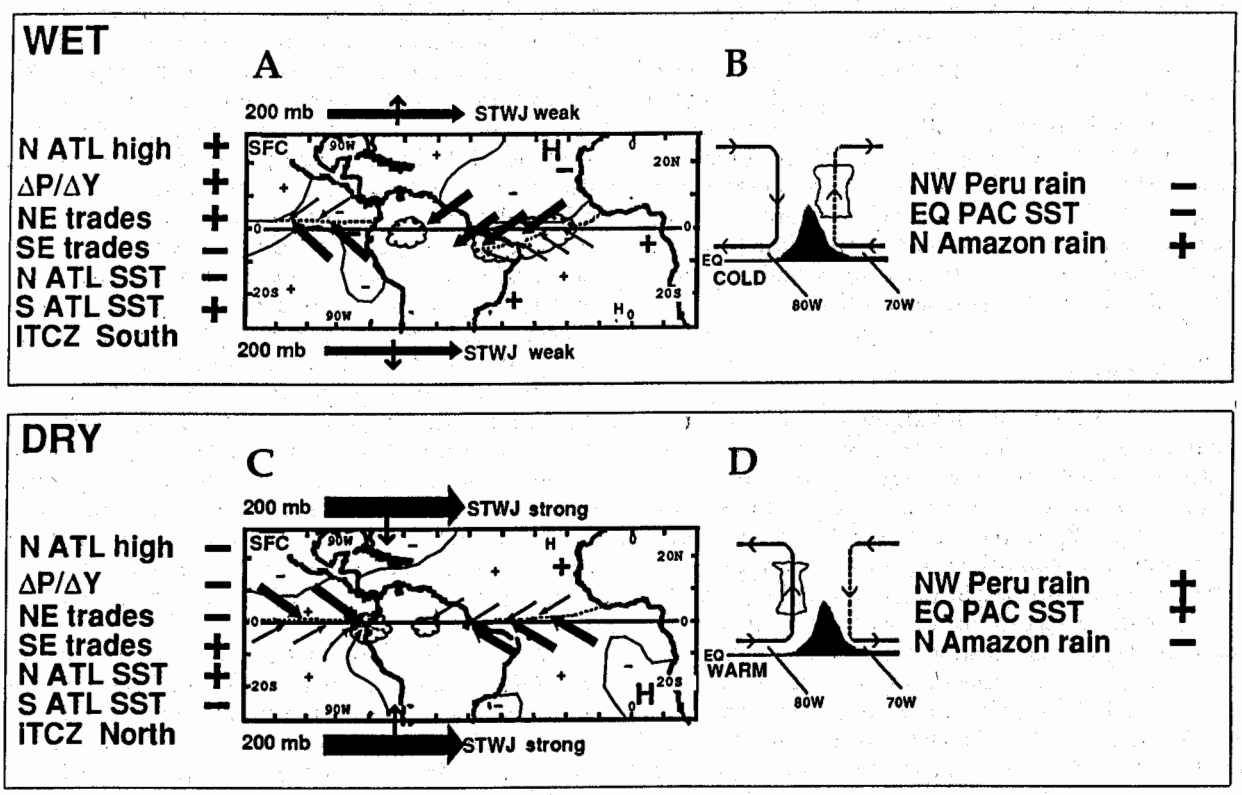

FIG. 9. Synthesis of surface circulation (a), (c) and zonal vertical cross section along the equator (b), (d) at the March–April rainy season peak in northern Amazonia during WET (a), (b) and DRY (c), (d) years. Broad/narrow arrows denote strong/weak trade winds in (a) and (c), heavy broken line wind confluence, bold/light letter H strong/weak North Atlantic high in (a), (c). Heavy solid lines separate areas of positive and negative SST anomalies, as indicated by large and small plus and minus signs inside the maps in (a) and (c). Solid/broken lines in (b) and (d) refer to the observed/hypothesized zonal-vertical circulation. Strong convective activity is indicated by scalloping in (a) and (c), and by vertical cloud symbols in (b) and (d).

lation sketched in Figs. 9b and 9d is from only two years in contrasting SO phases, and the rainfall anomalies in the Amazon basin are not prevailingly related to the SO. The mechanisms proposed in Fig. 9 appear operative around the rainy season peak in northern Amazonia, whereas relationships are not distinct in other seasons and the southern part of the basin. Finally, the study points to potentially important processes that have received little attention so far; in particular, the Amazon convection center of austral summer plausibly entails compensatory subsidence, and changes in intensity and location of this center of action may exert a control on the surface climate of adjacent regions of the continent.

Acknowledgments. This study was supported by NSF Grant ATM-9101097 and NOAA Grant NA26GP0088-01. Lawrence Greischar helped with the processing of the ECMWF and HRC data, and Carlos Nobre and Goki Tsuzuki provided hydrometeorological data from Brazil. We thank Pedro Silva Dias and an anonymous reviewer for helpful comments on an earlier version of this paper.

REFERENCES

Aceituno, P., 1988: On the functioning of the Southern Oscillation in the South American sector. Part I: Surface climate. *Mon. Wea. Rev.*, **116**, 505–524.

——, 1989: On the functioning of the Southern Oscillation in the South American sector. Part II: Upper-air circulation. *J. Climate*, **2**, 341–355.

Departamento Nacional de Aguas e Energia Elétrica, 1989: *Inventário das estações fluviométricas.* Divisão de Controle de Recursos Hídricos. 243 pp.

Dickinson, R., 1986: Climate, vegetation, and human interactions in the Amazon. *The Geophysiology of Amazonia*, R. Dickinson, Ed., Wiley, 1–9.

Figueroa, S. N., and C. A. Nobre, 1990: Precipitation distribution over central and western tropical South America. *Climanálise*, **5**, 36–45.

García, O., 1985: *Atlas of highly reflective clouds for the global tropics: 1971–1983.* NOAA-ERL, 365 pp. [Available from U.S. Superintendent of Documents, USGPO, Washington, D.C. 24402.]

Gruber, A., M. Varnadore, P. Arkin, and J. Winston, 1987: *Monthly and seasonal mean outgoing longwave radiation and anomalies.* NOAA Atlas no. 26, NOAA/NWS/NESDIS, U.S. Department of Commerce, 220 pp. [Available from Climate Analysis Center, NMC/NWS/NOAA, Washington, D.C. 20233.]

Hastenrath, S., 1990a: The relationship of highly reflective clouds to tropical climate anomalies. *J. Climate*, **3**, 353–365.

——, 1990b: Prediction of northeast Brazil rainfall anomalies. *J. Climate*, **3**, 893–904.

——, 1991: *Climate Dynamics of the Tropics.* Kluwef, 488 pp.
——, and P. Lamb, 1977: *Climatic Atlas of the Tropical Atlantic and Eastern Pacific Oceans.* University of Wisconsin Press, 113 pp.
——, L. C. de Castro, and P. Aceituno, 1987: The Southern Oscillation in the tropical Atlantic sector. *Contrib. Atmos. Physics,* **60,** 447–463.
Horel, J., and A. Cornejo-Garrido, 1986: Convection along the Coast of Northern Peru during 1983: Spatial and temporal variations of cloud and rainfall. *Mon. Wea. Rev.,* **114,** 2091–2105.
Hoskins, B., H. Hsu, I. James, M. Masutani, P. Sardeshmuk, and G. White, 1989: *Diagnostics of the global atmospheric circulation based on ECMWF analyses 1979–1989.* International Council of Scientific Unions, World Climate Program Research. WCRP-27, 217 pp. [Available from Dept. of Meteorology, University of Reading, Whiteknights, Reading RG6 2AU, United Kingdom.]
Janowiak, J., A. Krueger, P. Arkin, and A. Gruber, 1985: *Atlas of outgoing longwave radiation derived from NOAA satellite data.* NOAA Atlas no. 6, NOAA/NWS/NESDIS, U.S. Department of Commerce, 44 pp. [Available from Climate Analysis Center, NMC/NWS/NOAA, Washington, D.C. 20233.]
Kayano, M., T., V. Rao, and A. Moura, 1988: Tropical circulations and the associated rainfall anomalies during two contrasting years. *J. Climatol.,* **8,** 477–488.
Kousky, V., 1980: Diurnal rainfall variations in Northeast Brazil. *Mon. Wea. Rev.,* **106,** 488–498.
——, M. T. Kagano, and I. Cavalcanti, 1984: A review of the Southern Oscillation: Oceanic-atmospheric circulation changes and related rainfall anomalies. *Tellus,* **36A,** 490–504.
Marengo, J. A., 1992: Interannual variability of surface climate in the Amazon basin. *Int. J. Climatol.,* **12,** 853–863.
Meste, C., and M., 1991: Distribution spatio-temporelle des precipitations du domaine intertropical Sud-Americain a l'Est des Andes, moyenne 1931–1960. Université Paul Sabatier, Toulouse.
Molion, L. C. B., 1987: On the dynamic climatology of the Amazon basin and associated rain-producing mechanisms. Dickinson, R. E., Ed. *The Geophysiology of Amazonia,* Wiley, 391–407.
Moura, A. D., and M. T. Kagano, 1986: A distribuição da precipitação para os anos extremos do Nordeste do Brasil. *Rev. Bras. Meteorol.,* **1,** 1–10.
Nobre, C. A., P. J. Sellers, and J. Shukla, 1991: Amazonian deforestation and regional climate change. *J. Climate,* **4,** 957–988.
Obregón, G. O., and C. A. Nobre, 1990: Principal component analysis of precipitation fields over the Amazon river basin. *Climanálise,* **5,** 35–46.
Oort, A., Y. Pan, R. Reynolds, and C. Ropelewski, 1987: Historical trends in the surface temperature over the oceans based on the COADS. *Climate Dyn.* **2,** 29–38.
Philander, G., 1986: Unusual conditions in the tropical Atlantic Ocean in 1984. *Nature,* **322,** 236–238.
Rao, V. B., and K. Hada, 1990: Characteristics of rainfall over Brazil: annual variation and connections with the Southern Oscillation. *Theor. Appl. Climatol.,* **42,** 81–91.
Salati, E., A. Dall'Olio, E. Matsui, and J. Gat, 1979: Recycling of water in the Amazon basin: An isotopic study. *Wat. Resour. Res.,* **15,** 1250–1279.
Slutz, R., J., S. Lubker, J. Hiscox, S. Woodruff, R. Jenne, R., D. Joseph, P. Steurer, and J. Elms, 1985: Comprehensive Ocean-Atmosphere Data Set, Release 1. NOAA Environmental Research Laboratories, Climate Research Program, 268 pp.
Trenberth, K., and J. Olson, 1988: ECMWF analyses 1979–1986: Circulation statistics and data evaluation. NCAR/TN-300+STR, Climatic and Global Dynamics Division, 94 pp. [Available from NCAR.]